PCCP

Beyond the point defect limit: solid solutions, phase diagrams and trace-element partitioning†

M. Yu. Lavrentiev,*‡[a] N. L. Allan[a] and J. A. Purton[b]

[a] *School of Chemistry, University of Bristol, Cantock's Close, Bristol, UK BS8 1TS*
[b] *CLRC, Daresbury Laboratory, Warrington, Cheshire, UK WA4 4AD*

Received 6th January 2003, Accepted 20th March 2003
First published as an Advance Article on the web 8th April 2003

Traditionally disorder in solid oxides has largely been investigated theoretically *via* classical point defect theory; such methods are not readily extended to solid solutions, liquid phases or grossly non-stoichiometric compounds. In this paper we show how Monte Carlo simulations in the semigrand canonical ensemble, which include the explicit interchange of cations and use configurational bias techniques, are an attractive method for situations involving *finite* and even high concentrations of defects or foreign atoms. We illustrate our approach with two examples involving CaO: (i) the phase diagram for the system CaO–MgO is calculated for both solid *and* liquid phases. All the characteristic features are reproduced, including the eutectic point and the regions of liquid–solid coexistence; (ii) the first direct calculation of trace-element partitioning between solid and melt phases. Our techniques take full account of local structural distortion and clustering due to the mismatch between the sizes of the cations involved.

Introduction

Ceramic solid solutions, grossly non-stoichiometric oxides, and phase stability all present considerable challenges for theory. Oxide solutions are often strongly non-ideal. Energy differences between different phases are often small. Subtle cation ordering effects and resulting local changes in structure can often be crucial in determining phase stability and thermodynamic and chemical properties. An understanding of non-ideal behaviour and ordering is also key to any process in which there is a distribution of trace elements between two solid phases, or between solid and melt. Approaches such as the cluster variation method (CVM),[1] which are widely used for metallic alloys, often produce poor results when the species involved are markedly dissimilar, as usually occurs in oxides and minerals.

The importance of allowing for "relaxation" of the ions surrounding a defect in ionic solids, has long been recognized[2,3] Disorder in *solid* oxides has largely been investigated theoretically *via* point defect calculations[4] (the dilute limit) or *via* the use of 'supercells'.[5] In *point defect* calculations the total energy of the defective system is minimized by a relaxation of the nuclear positions and shell displacements of the ions surrounding the defect, which assumes the relaxation is greatest in the proximity of the defect and that relaxations decrease fairly rapidly away from the defect. The crystal is partitioned into two regions: an inner region immediately surrounding the defect, where relaxations are assumed to be greatest and elastic equations for the force are solved explicitly, and an outer region in which relaxations are estimated using a suitable approximation. In the "*supercell*" approach a superlattice of defects is introduced, which thus extends throughout the macroscopic crystal. The periodicity is then that of the particular superlattice chosen and convergence towards properties of an isolated defect occurs as the superlattice spacing is increased. Neither method is readily extended to solid solutions, liquid phases or disordered systems with a *finite* impurity or defect content far from the dilute limit.

We are currently developing new methods for such problems. A key feature of all of these is the need to sample many different arrangements of ions, allowing for the exchange of ions located at crystallographically inequivalent positions. Any method must also take into account the local environment of each ion and the local structural movements (relaxation), which accompany any exchange of ions and reduce considerably the energy associated with these exchanges. Local effects due to ion association or clustering should not be averaged out. Methods should be readily extendible to incorporate the effects of high pressure or thermal (vibrational) effects. The use of parameterised Hamiltonians (*e.g.*, of Ising type) is increasingly difficult beyond binary or pseudobinary alloys and so we have not resorted to any such approximate scheme. Instead we calculate the energy of each configuration in the simulation using interatomic interaction potentials.

In this paper we illustrate our methods by tackling two problems. The first is the CaO–MgO system where we consider the entire composition range as well as the dilute limits. This system is a particular challenge due to the large difference in ionic radius[6] between Ca^{2+} (1.00 Å) and Mg^{2+} (0.72 Å). We calculate the *entire* phase diagram, including liquid and solid phases. We continue examining the incorporation of divalent trace elements (impurities) in CaO solid and melt and hence the partitioning of these elements between these two solid phases. An understanding of trace element partitioning[7] is of considerable interest in geochemistry since trace element concentrations in igneous rocks and their constituent phases (minerals ± quenched melts) are widely used to develop and test petrogenetic models.[8] A prerequisite for using trace elements in this fashion is the accurate knowledge of the

† Presented at the 78th International Bunsen Discussion Meeting on "Complex Oxides: Defect Chemistry, Transport and Chemical Reaction", Vaals, The Netherlands, October 6–9, 2002.
‡ On leave from the Institute of Inorganic Chemistry, 630090 Novosibirsk, Russia.

 DOI: 10.1039/b300153a

This journal is © The Owner Societies 2003

partitioning behaviour of trace elements between minerals and co-existing melts.

Exchange-bias Monte Carlo

All Monte Carlo calculations use a box-size of 512 ions and 4×10^7 steps, following initial equilibration of 1×10^7 steps. All calculations in this paper are based on an ionic model using two-body potentials to represent short-range forces. The particular set of interaction potentials employed is that of Lewis and Catlow, first introduced in their study of the parent oxides[9] and subsequently employed by Ceder *et al.*[10]

We start with a Monte Carlo simulation (MC) in which there are *no* cation interchanges. Allowing random moves of randomly selected atoms takes account of vibrational effects. Both atomic coordinates and cell dimensions are allowed to vary during the simulation. During one step of the MC simulation an atomic coordinate or a lattice parameter is chosen at random and altered by a random amount. To determine whether the change is accepted or rejected, the usual Metropolis algorithm[11,12] is applied. The maximum changes in the atomic displacements and the lattice parameters are governed by the variables $r_{\max}$ and $v_{\max}$, respectively. The magnitudes of these parameters are adjusted automatically during the equilibration part of the simulation to maintain an acceptance/rejection ratio of approximately 0.3.

Thus, in these MC calculations at each step either an atom movement or a change of size of the simulation box is attempted. Almost always only one cation arrangement is sampled—the initial configuration, which is chosen at random. Consequently, for CaO–MgO, the calculated variation of ΔH_{mix} varies erratically with composition, and there is a strong dependence of ΔH_{mix} with the choice of initial arrangement. For a 50/50 mixture we were able, by choosing different cation arrangements, to vary ΔH_{mix} by as much as 40 kJ mol^{-1}. This is much higher than the final value of ΔH_{mix} obtained below.

We have described elsewhere[13] Monte Carlo Exchange (MCX) simulations in which *both* the atomic configuration *and* the atomic coordinates of all the atoms are changed. In any step, a random choice is made whether to attempt a random exchange between two atoms, a random displacement of an ion, or a random change in the volume of the simulation box. Again, the Metropolis algorithm is used to accept or reject any attempted move. This technique works well[14] for the MnO–MgO solid solution but for CaO–MgO, where there is a much larger mismatch between the cation radii, the rate of successful exchanges in MCX simulations is much smaller and amounts to only ≈1% of the attempted exchanges at 2000 K. Long runs are thus necessary in order to obtain good sampling of configurations. These are computationally far too expensive, and we must resort to special methods in order to increase the rate of successful exchanges.

To speed up the sampling of configurations, we apply the biased sampling technique, which is widely used in simulations of molecules with an orientation-dependent interaction potential (orientational bias) and polymer conformations (configurational bias),[12] to the CaO/MgO solid solution. In our exchange-bias Monte Carlo, instead of considering a single trial exchange, a set of trial exchanges is picked at random. One of these is then chosen as explained below. The acceptance rule differs from the standard Monte Carlo (Metropolis) algorithm. Below, we describe the exchange-bias Monte Carlo algorithm in detail and demonstrate that it satisfies the condition of detailed balance.

In our exchange-biased Monte Carlo,[15] instead of considering a single trial exchange, a set of trial exchanges is picked at random. Suppose an exchange takes place between atoms A and B. First, k pairs $\{A^i, B^i, i = 1,\ldots, k\}$ are randomly chosen. Here we set k equal to 100. We denote the system energy in the initial configuration as U_{old} and the energy of the system after exchange of atoms in the ith pair as U^i_{new}. One of the new configurations is then chosen with probability

$$p_i = \frac{\exp(-\beta(U^i_{\mathrm{new}} - U_{\mathrm{old}}))}{W_{\mathrm{new}}}, \beta = (kT)^{-1} \tag{1}$$

where W_{new} is given by

$$W_{\mathrm{new}} = \sum_{i=1}^{k} \exp[-\beta(U^1_{\mathrm{new}} - U_{\mathrm{old}})] \tag{2}$$

The chosen configuration i (*i.e.*, that after the exchange of the ith pair) with energy $U^i_{\mathrm{new}} \equiv U_{\mathrm{new}}$ is then the trial configuration. However, the usual acceptance rule cannot be directly applied. Instead, starting from the new configuration, a further $k-1$ pairs A^j, B^j, $j = 1,\ldots, k-1$ are chosen. Denoting the energy of the system after exchange of atoms in the jth pair U^j_{old}, we evaluate W_{old}, where

$$W_{\mathrm{old}} = \exp[-\beta(U_{\mathrm{old}} - U_{\mathrm{new}})] + \sum_{j=1}^{k-1} \exp[-\beta(U^j_{\mathrm{old}} - U_{\mathrm{new}})] \tag{3}$$

To fulfill detailed balance, the criterion for the acceptance of the new configuration is

$$\mathrm{acc}(\mathrm{old} \rightarrow \mathrm{new} = \min\left[1, \exp[-\beta(U_{\mathrm{old}} - U_{\mathrm{new}})]\frac{W_{\mathrm{new}}}{W_{\mathrm{old}}}\right] \tag{4}$$

The use of the exchange-bias technique increases the successful exchange rate of Ca^{2+} and Mg^{2+} in the CaO–MgO solid solution from ≈1% to ≈45%. at 2000 K. This rate of exchange is sufficient for convergence for the systems and properties we examine in this paper.

Chemical potential and the semigrand-canonical ensemble

Simulations were performed using the semigrand-canonical ensemble[12,16] at temperatures between 2000 and 4000 K and zero pressure monitoring the enthalpy and volume of the system and the chemical potential difference between Ca^{2+} and Mg^{2+} ions. The latter was calculated as previously implemented by us[15] for the determination of the phase diagram of the solid phases of MgO–MnO. In this method we evaluate the potential energy change $\Delta U_{\mathrm{B/A}}$ which would result if one species, B, were to be converted into another, A. This change in energy is related to the corresponding change in chemical potential $\Delta\mu_{\mathrm{B/A}}$ by

$$\Delta\mu_{\mathrm{B/A}} = -kT \ln\left\langle \frac{N_{\mathrm{B}}}{N_{\mathrm{A}} + 1} \exp(-\Delta U_{\mathrm{B/A}}/kT) \right\rangle \tag{5}$$

Thus for CaO–MgO, we evaluate the energy associated with the conversion of a randomly chosen Mg^{2+} ion to Ca^{2+}, $\Delta U_{\mathrm{Mg/Ca}}$, every fifth step (on average). As the simulation proceeds, the average value of the right hand side of eqn. (5) is determined. Note that the change of Mg into Ca is only considered but *not* actually performed—the configuration remains unchanged after evaluating $\Delta U_{\mathrm{Mg/Ca}}$. We have checked consistency in that identical results are obtained considering the reverse transformation, *i.e.*, of a randomly chosen Ca^{2+} to a Mg^{2+}.

At $T \approx 3000$ K the system begins to melt. The liquid–solid transition is evident in a plot of volume *vs.* temperature, with a characteristic jump at the melting point. It is well known that it is difficult to locate melting points exactly in Monte Carlo and molecular dynamics simulations if the initial system is homogeneous, because of significant overheating.[17–19] In our Monte Carlo calculations the calculated melting temperature is also too high if the starting configuration is the one

appropriate for a solid phase. If instead, the simulations start from the liquid phase, the system does not crystallize at low temperatures, but rather freezes into a glass-like state. In order to avoid this hysteresis and establish the melting point, we start simulations using a simulation box that is half-solid, half-liquid. This strategy has been used successfully previously in molecular dynamics simulations (of, *e.g.*, forsterite,[20] $MgSiO_3$[21] and MgO[22]). In our case, we started by performing simulations at a very high temperature (4500 K), where the system is molten for all Ca/Mg concentrations. Then, half of the simulation box was filled using a configuration appropriate for the melt, and the other half with perfect solid crystal. We tried different ways of constructing this initial half-melt, half-solid configuration by locating the interface between the two at either the (100) or the (110) solid surface. The results from each are virtually identical. In this way the location of the melting point can then be determined to within a few degrees. The calculated melting temperatures T_m for pure MgO and pure CaO are 2870 K and 2600 K, respectively. For both systems, calculated temperatures are 10–15% lower than experiment[23,24] but it is encouraging that our calculated melting point for CaO is less than that of MgO. Overall agreement is very satisfactory, particularly bearing in mind that the potentials were originally fitted to reproduce a range of solid-state properties only in the static limit.[9]

Phase diagram

Given the dependence of the chemical potential difference $\Delta\mu = \mu_{Ca} - \mu_{Mg}$ on concentration, the thermodynamic potential and hence the phase diagram of the system can be determined. In practice, this problem is more complicated here than in our earlier work on solid solutions[13] due to the existence of the liquid phase. At temperatures where solid and liquid phases coexist, a plot of $\Delta\mu(x_{Mg})$ *vs.* x_{Mg} contains regions corresponding to solid and to liquid, depending on which phase has the lower thermodynamic potential at any given concentration, as illustrated in Fig. 1. To extract the phase diagram from the simulations, it is necessary to find the thermodynamic potential for *both* phases. The coexistence concentrations can then be found from the usual double tangent construction.

The calculated values of $\Delta\mu(x_{Mg})$ were fitted to a cubic polynomial in x_{Mg} similar in form to that used in the Margules approximation for solid solutions:[25]

$$\frac{\Delta\mu_{s(l)}}{kT} = \ln\frac{x}{1-x} + a_{s(l)} + b_{s(l)}x + c_{s(l)}x^2 + d_{s(l)}x^3 \qquad (6)$$

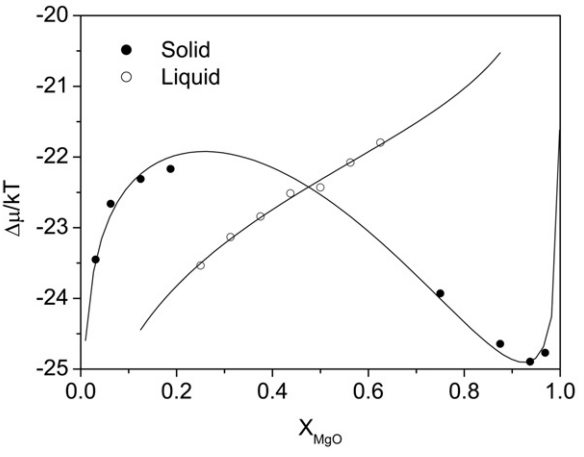

Fig. 1 Chemical potential *vs.* composition for CaO–MgO at 2500 K. Solid and empty circles denote solid and liquid phases, respectively.

where s(l) refers to solid (liquid) phase and we have dropped the Mg subscript for clarity. The cubic term was found to be negligible for the liquid phase, but it is important to keep this term for the solid phase to describe the asymmetry of the calculated $\Delta\mu_s$. Integrating with respect to x_{Mg} gives $G(x_{Mg})$:

$$\frac{G_{s(l)}}{kT} = x\ln x + (1-x)\ln(1-x) + a_{s(l)}x + \frac{1}{2}b_{s(l)}x^2 + \frac{1}{3}c_{s(l)}x^3 + \frac{1}{4}d_{s(l)}x^4 + C_{s(l)} \qquad (7)$$

for both phases. The last unknown parameter for both phases is the constant $C_{s(l)}$, which depends only on temperature; in fact, only the difference between these constants $C_s - C_l$ is required to compare the free energy of solid and liquid phases. When $x_{Mg} = 0$ (pure CaO), then at the calculated melting point, 2600 K, the free energies of both phases are equal and $C_s - C_l = 0$. Similarly, at $T = 2870$ K (the calculated melting point of pure MgO), the free energies of liquid and solid are equal when $x_{Mg} = 1$, from which we can obtain the value of $C_s - C_l$. We assume $C_s - C_l$, which we need only over a 500 K temperature range, varies linearly with T. We have checked this is a good approximation by also extracting the value of $C_s - C_l$ at 2400 K where $\Delta\mu(x_{Mg})$ also jumps between solid and liquid phases when $x_{Mg} = 0.26$. This provides all the information required to determine the phase diagram.

Fig. 2a shows the calculated enthalpy of mixing of solid CaO/MgO as a function of composition at 2000 K and the enthalpy of mixing liquid CaO/MgO at $T = 3000$ K. The

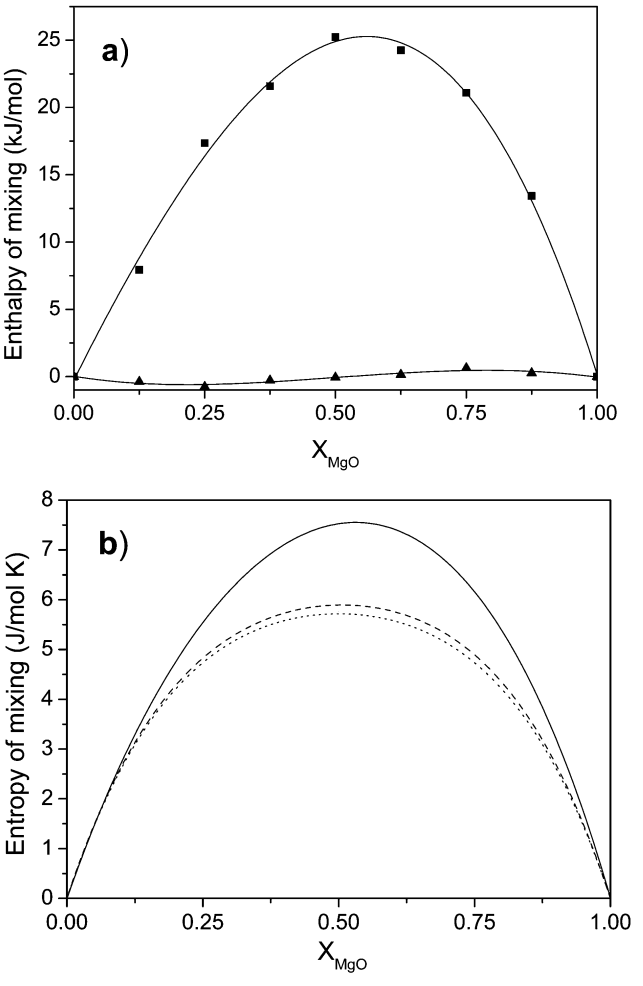

Fig. 2 (a) ΔH_{mix} (kJ mol^{-1}) at 2000 K (solid state, circles) and 3000 K (liquid state, triangles). (b) ΔS_{mix} (J mol^{-1} K^{-1}) at 2000 K (solid state, full line) and $T = 3000$ K (liquid state, dashed line). The ideal entropy of mixing is also shown (dotted line).

curve for the solid system is somewhat asymmetric, with a maximum ≈25 kJ mol^{-1} when the mole fraction of MgO is ≈0.54. Our results for ΔH_{mix} are substantially lower than those of Ceder and co-workers[10] who used the same set of potentials and, for example, predict enthalpies as high as ≈49 kJ mol^{-1} for an equimolar mixture of CaO and MgO. This difference may result from the use in ref. 10 of ordered cation arrangements and relatively small unit cells (up to 64 ions). As shown above, in the absence of exchanges the results for ΔH_{mix} in Monte Carlo can be substantially higher, closer to the results by Ceder *et al.*[10] We have previously evaluated,[26] enthalpies of mixing in the solid state for *small* CaO concentrations up to $x_{Ca} = 0$ using hybrid Monte Carlo and quasiharmonic lattice dynamics methods. The results obtained here are in good agreement with these previous data. We also note in passing that the energy associated with the replacement of a single Ca by a Mg or of a single Mg by a Ca varies significantly with composition. For the liquid system, ΔH_{mix} is close to zero, indicating virtually ideal behaviour.

Entropies of mixing can be extracted from the free energies and enthalpies of mixing. Values of ΔS_{mix} at 2000 K and 3000 K are shown in Fig. 2b together with the ideal entropy of mixing. The excess entropy in the solid state can be as high as 30% of the ideal entropy, which is substantially higher than that calculated[13] for MgO–MnO. As with the excess enthalpy, there is a slight asymmetry in the entropy *vs.* composition curve. These results are also in good agreement with those obtained using our configurational lattice dynamics approach to solid solutions;[26] however these lattice dynamics calculations were restricted to compositions <16% CaO since at higher CaO concentrations the quasiharmonic approximation broke down, preventing full free energy minimisation. Although ΔH_{mix} for CaO/MgO is large and positive, it is clear that this is offset in the single-phase regions by large, positive values of ΔS_{mix}, which are considerably in excess of the 'ideal' value. In contrast, in the melt (3000 K) ΔS_{mix} is much smaller than in the solid, again indicating that the solution is close to ideal.

The calculated dependence of $\Delta G(x_{Mg})$ at four different temperatures is shown in Fig. 3. At 2400 K the system is solid at all concentrations (Fig. 3a): the straight line (common tangent) defining the two phase region does not intersect the dashed line showing the calculated free energy of the liquid phase. At 2440 K (Fig. 3b) this common tangent is also a tangent to the liquid-phase curve, and so all three phases coexist at this temperature (the eutectic point). The concentration of Mg in the liquid phase is 0.32. For comparison, the experimental value[23] of $T^{eutectic}$ is 2647 K, at a Mg mole fraction, $x_{MgO}^{eutectic} = 0.41$. At a higher temperature, 2500 K, the liquid phase coexists with one of the two solid phases, depending on the overall composition of the system (Fig. 3c). At higher temperatures still, the liquid curve lies below the solid curve and there is liquid at all compositions.

The resulting phase diagram is shown in Fig. 4. The overall agreement with the experimental phase diagram is good. All the characteristic features of the MgO/CaO phase diagram, including the eutectic point and the regions of liquid–solid coexistence, are reproduced. We predict that solid MgO is more soluble in solid CaO than CaO in MgO, in agreement with the experiments of Doman *et al.*[23] and of Trojer and Konopicky.[27]

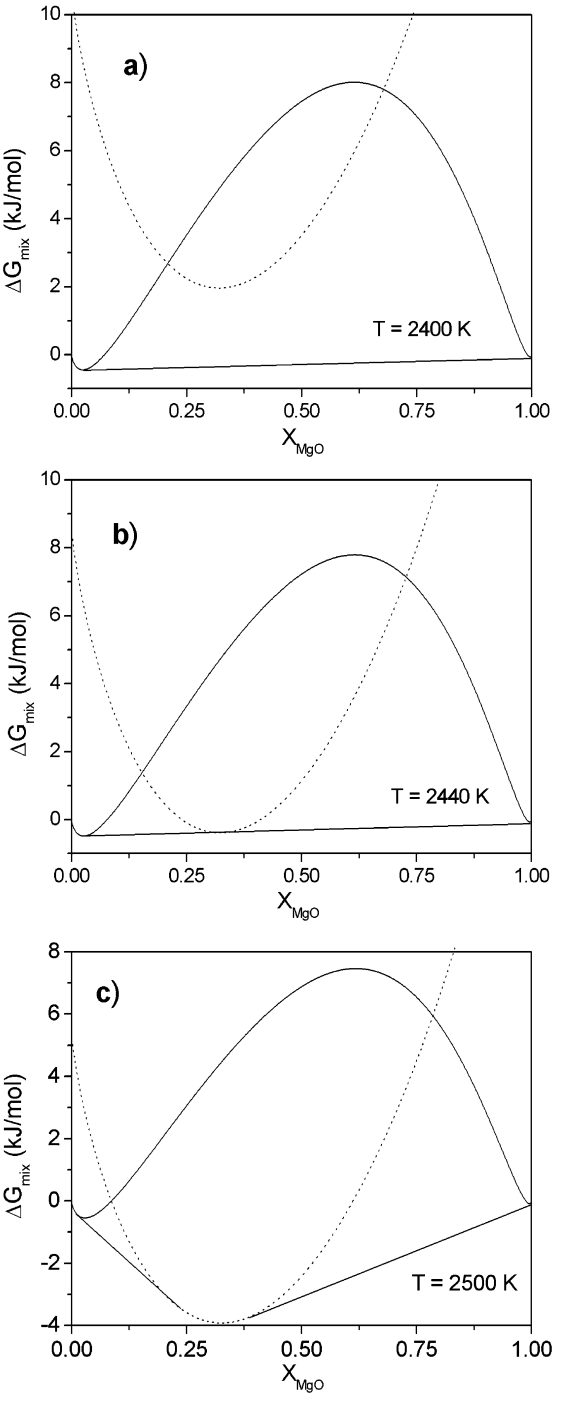

Fig. 3 ΔG_{mix} *vs.* composition at (a) 2400 K, (b) 2440 K (c) 2500 K. Solid lines correspond to the solid phase, dashed lines to the liquid phase.

Trace element partitioning

We can extend the approach outlined in previous sections to a further problem—the *direct* calculation of the partitioning of a trace element or dopant between more than one phase. Our knowledge of the accretion and subsequent chemical differentiation of the Earth, for example, derives largely from chemical analyses of trace elements and their isotopes in rocks; modelling and interpretation of these data require an understanding of how trace elements are partitioned between coexisting phases. Here we consider partitioning of a range of divalent trace element cations J (J = Ni^{2+}, Mg^{2+}, Fe^{2+}, Mn^{2+} and Sr^{2+}) between the solid and melt phases of CaO. Previous approaches to this quantity have generally ignored the liquid phase[7,28] or worked only with enthalpies of substitution in each phase in the dilute limit and ignored entropic contributions.[29,30] To our knowledge, this is the first full *direct* calculation of partition coefficients between mineral and melt. Our method is quite general.

We adopt the usual convention[7] that the partition coefficient D is the ratio of the molar concentrations of the trace element in the solid to that in the liquid phase and so equal to x_s/x_l.

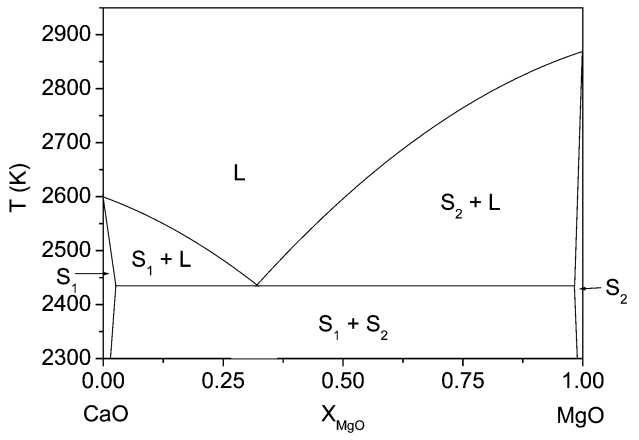

Fig. 4 Calculated phase diagram of CaO/MgO. S_1 denotes solution of MgO in solid CaO, S_2 solution of CaO in solid MgO, L corresponds to the liquid mixture of both components. $S_1 + L$, $S_2 + L$, $S_1 + S_2$ are regions of coexistence of the two phases.

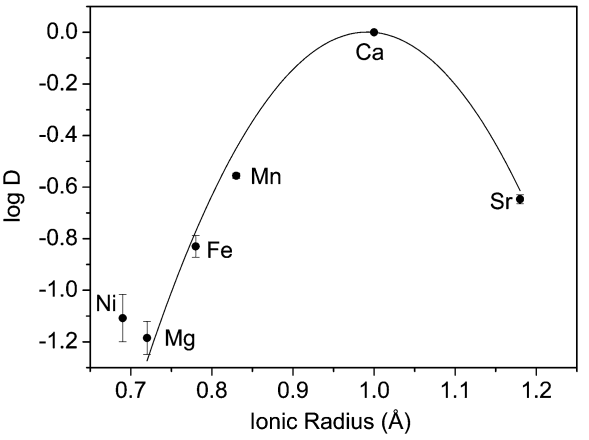

Fig. 6 Calculated partition coefficients at 2600 K of a range of divalent cations between CaO solid and melt phases as a function of ionic radius.

Small values of D correspond to trace elements that prefer the melt to the solid phase. As shown schematically in Fig. 5a, the partition coefficient at any temperature can be found from the phase diagram of the CaO–JO system where J is the trace element of interest. A schematic plot of the dependence of the free energy of solid and liquid mixtures on the concentration of the trace elements is given in Fig. 5b. The partition coefficient can be determined from the usual double tangent construction, as shown also in this figure.

The starting point for our calculations is once again the expression for the chemical potential difference as a function of concentration [Fig. 1 and eqn. (6)]. We run semigrand canonical simulations at the required temperature for both liquid and solid systems (CaO–JO), as described earlier. The resulting values of $\Delta\mu_{B/A}$ for solid and liquid are fitted separately to eqn. (6).

At equilibrium, the chemical potentials of both A and B must be the same in both phases. Thus the difference in chemical potential ($\Delta\mu_{B/A}$, eqn. (6)) must also be the same in both solid and melt phases. From eqn. (6) it follows that

$$a_s - a_l = \ln(x_L(1 - x_S)/x_S(1 - x_L)) + b_l x_L - b_S x_S + c_l x_L^2 - c_S x_S^2 + d_L x_L^3 - d_s x_S^3 \quad (8)$$

When x_L and x_S are small, eqn. (8) simplifies to

$$a_l - a_s = \ln(x_S/x_l) \quad (9)$$

and the partition coefficient D is given by

$$D = x_s/x_l = \exp(a_l - a_s) \quad (10)$$

Calculated partition coefficients are plotted in Fig. 6 as a function of ionic radius. D varies over more than an order of magnitude over the range of cations we have examined. Unfortunately there does not appear to be direct experimental data for comparison. Nevertheless, a large number of experimental studies on a wide range of minerals[31–33] indicate that partition coefficients for isovalent series of cations show an approximately parabolic dependence on ionic radius. The optimum radius, *i.e.*, that for which D is largest, lies close to the radius

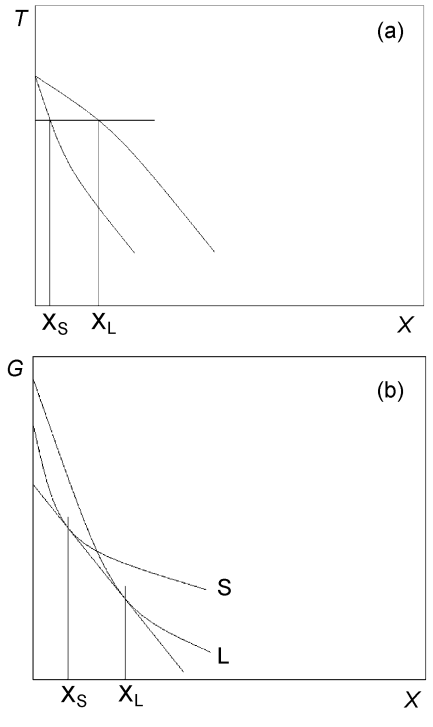

Fig. 5 (a) Schematic phase diagram of a binary oxide system near the melting point. The partition coefficient D is given by $D = X_S/X_L$. (b) Schematic plot of the free energies of solid and liquid solutions at small impurity concentrations.

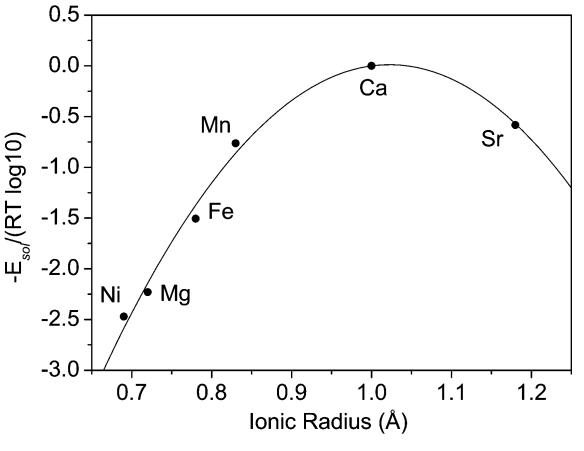

Fig. 7 Solution energies (in the static limit) of a range of divalent cations in solid CaO as a function of ionic radius. For more details, see the text.

of the host cation in the solid. The calculations reproduce the characteristic parabolic shape observed experimentally with a maximum close to the ionic radius of Ca^{2+}. It is interesting that the calculated partition coefficient of Ni^{2+} is larger than that of Mg^{2+} although it has a smaller ionic radius and is thus somewhat out of line with the general trend.

For comparison, in Fig. 7 we plot the solution energy E_{sol} (as $-E_{sol}/RT$ log10 for direct comparison with Fig. 6) of the binary oxides JO (J = Ni^{2+}, Mg^{2+}, Fe^{2+}. Mn^{2+} and Sr^{2+}) in solid CaO. These are calculated, in the static limit, from the point defect energy E_{def} (J_{Ca}) associated with the substitution of a Ca^{2+} by J^{2+}, and the lattice energies E_{latt} of CaO and JO. Using Kröger–Vink notation,

$$\mathrm{JO(s)} + \mathrm{Ca_{Ca}} \rightarrow \mathrm{J_{Ca}} + \mathrm{CaO(s)}$$
$$E_{sol} = E_{def}(\mathrm{J_{Ca}}) + E_{latt}(\mathrm{CaO}) - E_{latt}(\mathrm{JO}) \qquad (11)$$

The variation of these solution energies with ionic radius is similar to that of the partition coefficients in that the curve is approximately parabolic with maximum solubility, as expected, at an ionic radius close to that of Ca^{2+}. The variation of the solution energy with size is nevertheless greater than that of the partition coefficients, as is evident from the larger curvature of the parabola in Fig. 7. In contrast to the behaviour of the partition coefficients, the solution energy of Ni^{2+} is larger than that of Mg^{2+} in keeping with their relative ionic radii. Nevertheless, the solution energy of Ni^{2+} is smaller than expected from a parabolic extrapolation from those of the larger ions. In passing, it is worth noting that equations of the form of eqn. (11) have been used[34] to rationalise trace-element partitioning since as long ago as 1927.

Finally we relate our results briefly to an approximate model for trace-element partitioning commonly used by geochemists to fit experimental data. Proposed by Blundy and Wood,[32] this links the partition coefficient to the Young's modulus of the solid crystal, E. In this model,

$$D = D_0 \exp\left(\frac{-4\pi E\left\{\frac{r_0}{2}(r_j - r_0)^2 + \frac{1}{3}(r_j - r_0)^3\right\}}{kT}\right) \qquad (12)$$

where r_j is the ionic radius of the substituent cation, r_0 the optimum radius of the site of interest and D_0 the maximum value of D. We have fitted our calculated partition coefficients to eqn. (12). The resulting fitted value of E is ≈250 GPa. In contrast, using the same set of interionic potentials, the calculated Young's modulus of solid CaO in the static limit is only 149 GPa. Furthermore the Young's modulus decreases with increasing temperature. We have also fitted the calculated solution energies, rather than the partition coefficients themselves, to an equation of the form of eqn. (12), obtaining an effective E ≈420 GPa. The functional form of eqn. (12) does appear to be reasonable in describing the variation of D from one element to another, but the resulting values of E are best regarded only as effective moduli.

Conclusions

We have shown in this paper how exchange-bias Monte Carlo may be used to calculate the phase diagram of binary oxides for both melt and solid phases, and thus the partition coefficient of trace elements between these two phases. The calculated MgO/CaO phase diagram reproduces all the characteristic features of the experimental phase diagram, including the eutectic point and the regions of liquid–solid coexistence. A major advantage of our exchange-bias Monte Carlo approach over lattice dynamics and CVM is that it is also applicable to the liquid phase.

The key feature of our methods which are applicable to any composition is that they sample many configurations, explicitly considering different arrangements of ions, and allow for the *local* structural relaxation surrounding each cation. This relaxation is crucial. If ignored, the energy of exchange of any two ions is usually very high and all exchanges are rejected, thus sampling only one arrangement. Vibrational effects are included and the approach can be used at any pressure and temperature.

Acknowledgements

This work was funded by EPSRC grant GR/M53899 and two HEFCE JREI awards. Jon Blundy is thanked for helpful discussions.

References

1 *E.g.*, D. de Fontaine, *Solid State Phys.*, 1994, **47**, 33.
2 N. F. Mott and M. T. Littleton, *Trans. Faraday Soc.*, 1938, **34**, 485.
3 *E.g.*, A. B. Lidiard, *J. Chem. Soc., Faraday Trans. 2*, 1989, **85**, 541.
4 *E.g.*, C. R. A. Catlow and W. C. Mackrodt, *Computer Simulation of Solids*, C. R. A. Catlow and W. C. Mackrodt, ed., Berlin, Springer-Verlag, 1982, ch. 1.
5 *E.g.*, M. B. Taylor, G. D. Barrera, N. L. Allan, T. H. K. Barron and W. C. Mackrodt, *Faraday Discuss.*, 1997, **106**, 377.
6 All ionic radii in this paper for sixfold coordination are taken from R. D. Shannon, *Acta Crystallogr.*, 1976, **A32**, 751.
7 For a review see N. L. Allan, J. D. Blundy, J. A. Purton, M. Yu. Lavrentiev and B. J. Wood, *Solid Solutions in Silicate and Oxide Systems of Geological Importance*, ed. C. A. Geiger, vol. 3, European Mineralogical Union Notes in Mineralogy, series editors G. Papp and T. G. Weiszburg, Eötvös University Press, Budapest, 2001, ch. 11.
8 *E.g.*, D. McKenzie and R. K. O'Nions, *J. Petrol.*, 1991, **32**, 1021; K. Putirka, *J. Geophys. Res.*, 1999, **104**, 2817.
9 G. V. Lewis and C. R. A. Catlow, *J. Phys. C: Solid State Phys.*, 1985, **18**, 1149.
10 P. D. Tepesh, A. F. Kohan, G. D. Garbulsky, G. Ceder, C. Coley, H. T. Stokes, L. L. Boyer, M. J. Mehl, B. P. Burton, K. Cho and J. Joannopoulos, *J. Am. Ceram. Soc.*, 1996, **79**, 2033; A. F. Kohan and G. Ceder, *Phys. Rev. B*, 1996, **54**, 805.
11 N. I. Metropolis, A. W. Rosenbluth, M. N. Rosenbluth, A. H. Teller and E. Teller, *J. Chem. Phys.*, 1953, **21**, 1087.
12 D. Frenkel and B. Smit, *Understanding Molecular Simulation*, Academic Press, San Diego-London, 2nd edn., 2002.
13 J. A. Purton, G. D. Barrera, N. L. Allan and J. D. Blundy, *J. Phys. Chem. B*, 1998, **102**, 5202.
14 N. L. Allan, G. D. Barrera, M. Yu. Lavrentiev, I. T. Todorov and J. A. Purton, *J. Mater. Chem.*, 2001, **11**, 63.
15 M. Yu. Lavrentiev, N. L. Allan, G. D. Barrera and J. A. Purton, *J. Phys. Chem. B*, 2001, **105**, 3594.
16 D. A. Kofke and E. D. Glandt, *Mol. Phys.*, 1988, **64**, 1105.
17 K. J. Smolander, *Phys. Scr.*, 1990, **42**, 485.
18 M. Matsui and G. D. Price, *Nature*, 1991, **351**, 735.
19 B. Kapusta and M. Guillope, *Phys. Earth Planet. Inter.*, 1993, **75**, 205.
20 J. D. Kubicki and A. C. Lasaga, *Am. J. Sci.*, 1992, **292**, 153.
21 A. B. Belonoshko, *Geochim. Cosmochim. Acta*, 1994, **58**, 4039.
22 A. B. Belonoshko and L. S. Dubrovinsky, *Am. Mineral.*, 1996, **81**, 303.
23 R. C. Doman, J. B. Barr, R. N. McNally and A. M. Alper, *J. Am. Ceram. Soc.*, 1963, **46**, 313.
24 *Concise Encyclopedia of Chemistry*, Walter de Gruyter, Berlin–New York, 1994.
25 *E.g.*, J. B. Thompson, *Researches in Geochemistry*, P. H. Abelson, ed. John Wiley, New York, 1967, vol. II, p. 340.
26 N. L. Allan, G. D. Barrera, J. A. Purton, C. E. Sims and M. B. Taylor, *Phys. Chem. Chem. Phys.*, 2000, **2**, 1099.
27 F. Trojer and H. Konopicky, *Radex Rundsch.*, 1949, **4**, 16.

28 *E.g.*, J. A. Purton, N. L. Allan, J. D. Blundy and E. A. Wasserman, *Geochim. Cosmochim. Acta*, 1996, **60**, 4977.
29 M. Kanzaki, in *Physics meets mineralogy*, ed. H. Aoki, Y. Syono and R. J. Hemley, Cambridge University Press, Cambridge, 2000, ch. 6.4, pp. 381–389.
30 J. A. Purton, J. D. Blundy and N. L. Allan, *Am. Mineral.*, 2000, **85**, 1087.
31 N. Onuma, H. Higuchi, H. Watika and H. Nasagawa, *Earth Planet. Sci. Lett.*, 1968, **5**, 47.
32 J. D. Blundy and B. J. Wood, *Nature*, 1994, **372**, 452.
33 *E.g.*, W. van Westrenen, N. L. Allan, J. D. Blundy, J. A. Purton and B. J. Wood, *Geochim. Cosmochim. Acta*, 2000, **64**, 1629.
34 L. M. Henderson and F. C. Kracek, *J. Am. Chem. Soc.*, 1927, **49**, 739.